CrystEngComm

Accepted Manuscript

This article can be cited before page numbers have been issued, to do this please use: A. Koryáková, A. Chatziadi, J. Rohlíek, E. Zmeškalová, J. Beránek and M. Soos, *CrystEngComm*, 2025, DOI: 10.1039/D4CE01314J.

ROYAL SOCIETY OF CHEMISTRY

rsc.li/crystengcomm

View Article Online
DOI: 10.1039/D4CE01314J

Stability Study and Structural Insights into Cannabidiol Cocrystals

Adéla Koryťáková[1], Argyro Chatziadi[1], Jan Rohlíček[2], Eliška Zmeškalová[1,2], Josef Beránek[3], Miroslav Šoóš[1]

[1]Department of Chemical Engineering, University of Chemistry and Technology in Prague, Technická 3, 16628, Prague 6, Czech Republic

[2]Institute of Physics of the Czech Academy of Sciences, Na Slovance 2, 182 00, Prague 8, Czech Republic

[3]Zentiva k.s., U Kabelovny 130, 10237, Prague 10, Czech Republic

Abstract

Cannabidiol (CBD) is a non-psychoactive compound derived from cannabis and has attracted considerable attention due to its potential therapeutic benefits. It is increasingly used in various health-related products, including dietary supplements, because of its positive effects on pain relief, antioxidative properties, and protection against cell damage. Despite its promising applications, CBD faces significant challenges for oral administration, primarily due to its low solubility, low melting point (67 °C), and poor stability. In this work we used various methods for CBD cocrystal preparation to improve properties of CBD. We succeeded in preparing five cocrystals, which were fully characterized using several analytical tools, such as X-ray powder diffraction, differential scanning calorimetry, nuclear magnetic resonance. Notably, the cocrystals

View Article Online
DOI: 10.1039/D4CE01314J

increased their melting points compared to pure CBD. Furthermore, the intrinsic dissolution rate was measured for pure CBD and the multicomponent forms to describe the rate of release of CBD from the cocrystal. Finally, the crystal structures of three cocrystals were used to interpret the stability and degradation behaviour of the CBD cocrystals under accelerated conditions. Remarkably, the cocrystals CBD-4,4′-bipyridine and CBD-L-proline remained stable and unaffected for longer period under the stressed conditions compared to the pure CBD. This study provides valuable insight into the stability behaviour of the cocrystals under various conditions.

Key words: cannabidiol, cocrystal, characterization, dissolution, stability, chemical degradation

1 Introduction

Phytocannabinoids which are naturally occurring compounds in the Cannabis sativa plant (which is commonly known as hemp), have been used for a long time as a medicine for the treatment of pain, nausea, and insomnia.[1,2] They are a wide group of phytochemicals consisting of approximately 70 compounds, including the well-known psychoactive compound tetrahydrocannabinol (THC), as well as non-psychoactive cannabigerol (CBG), cannabinol (CBN), cannabichromene (CBC) and cannabidiol (CBD). The cannabis plant also contains other natural compounds such as flavonoids, alkaloids, and terpenes, which may influence the biological activity of the plant.[2,3]

CBD has emerged as a promising compound due to its non-psychoactive nature and therapeutic potential. Its mechanism of action, mediated by the endocannabinoid system, plays a crucial role in pain and inflammation modulation[4] and it has been shown to reduce spasticity in animal models.[5] Furthermore, it has additional benefits in treating insomnia, anxiety, depression, autism,

View Article Online
DOI: 10.1039/D4CE01314J

rheumatoid arthritis, and neurodegenerative disorders.[5,6] Despite all possible medical benefits, CBD has limited pharmaceutical formulations available. Notable examples of the only formulations approved by FDA and EMA are Epidiolex[7] (a sesame oil solution) and Sativex[8], (an alcohol-based spray containing CBD and THC in a 1:1 ratio). However, other strategies to improve CBD bioavailability have been suggested, including self-emulsifying drug delivery systems[9], intranasal sol-gels[10] and cyclodextrins complexes.[11] The lack of solid dosage forms of CBD represents a significant gap in the market, particularly given their advantages in patient convenience, compliance, dosing precision, and stability.[12,13]

The development of oral solid-state forms for CBD faces considerable challenges. The main limitations are its high lipophilicity (logP 6.3) and low solubility in water (12.6 mg/l), which lead to poor oral bioavailability.[1,10,14,15] Previous studies have explored strategies like salt formation[16] amorphous solid dispersion[17,18], and polymorphism[19] to address these issues, with mixed success. For example, while salts improved the dissolution profiles, they faced significant stability problems, requiring storage at lower temperatures under a nitrogen atmosphere. Furthermore, the new CBD polymorph exhibited a melting point around 43–46 °C, which is lower than the CBD stable form with melting point at 67 °C. Finally amorphous solid dispersions were stable only for 3 months, so they were not suitable for long term stability.[17,18]

Cocrystallization has emerged as a promising strategy to enhance the physicochemical properties of active pharmaceutical ingredients (APIs), including solubility, dissolution rate and stability.[20-22] Cocrystals are crystalline systems, which consist of two or more components in a defined stoichiometric ratio.[20,23] Cocrystals used in pharmaceutical industry are called pharmaceutical cocrystals and they are multicomponent forms formed by pharmaceutical active ingredient (API)

View Article Online
DOI: 10.1039/D4CE01314J

and usually inactive and pharmaceutically acceptable compound (Generally Recognized as Safe, GRAS). The molecules of a cocrystal are bonded by non-bonding interactions, such as hydrogen bonding, van der Waals forces, or π-π interactions. In the case of CBD , there are five cocrystals mentioned in the patent literature[24,25], namely, CBD-4,4′-bipyridine (BP), CBD-betaine (BE), CBD-L-carnitine (CR), CBD-L-proline (PR) and CBD-tetramethylpyrazine (TMP). However, these cocrystals have not been studied extensively, with the exception of CBD-TMP cocrystal which is currently undergoing nonclinical phase of pharmaceutical development known as ART 12.11 targeting treatment of anxiety disorders.[26,27]

Besides the low bioavailability challenges, CBD faces also stability problems particularly under exposure to light, heat and acidic or basic environment[6,28-30], which is also an important aspect for further pharmaceutical drug development. While stability studies on CBD solutions and oil-based formulations have provided valuable insights, there is limited information on the stability of solid-state CBD and its cocrystals.[6,31-34] Existing study suggests that the stability of CBD in its solid-state form is more influenced by heat than by humidity.[35]

This study addresses these gaps by focusing on the stability and physicochemical characterization of CBD cocrystals. Our first goal was to perform an extensive cocrystal screening to identify new CBD cocrystals with improved physicochemical properties. From this screening, one new cocrystal was synthesized with piperazine (PI), which has not been previously reported in the patent literature. In addition, we re-synthesised the known cocrystals (CBD-BP, CBD-CR, CBD-PR, CBD-BE, CBD-TMP) with the purpose to investigate more extensively their physicochemical properties and behaviour. The chemical structure of CBD and the corresponding coformers that lead to cocrystals formation are shown in Figure 1.

View Article Online
DOI: 10.1039/D4CE01314J

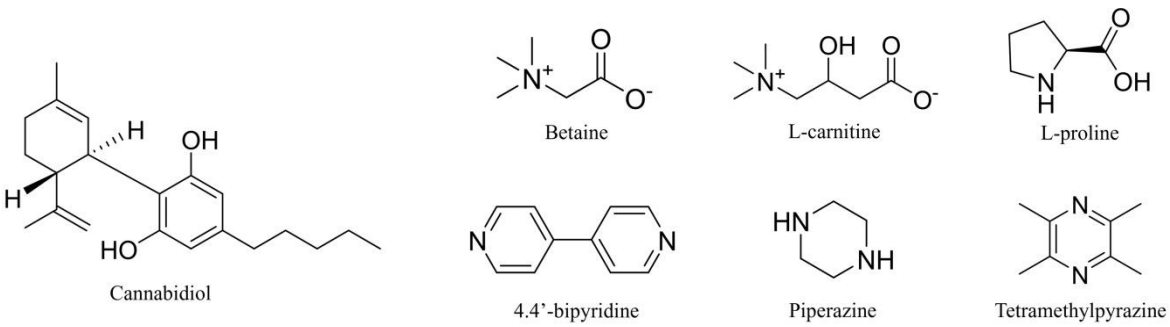

Figure 1. Structures of cannabidiol and its coformers that create cocrystals.

To gain a deep insight into their stability and understand better their behaviour, the characterization included their crystal structure determination (for CBD and three cocrystals, that it was possible) and interaction energy calculations. Furthermore, we conducted a dissolution study for the cocrystals and pure CBD using intrinsic dissolution rate measurement to describe their dissolution profile from the cocrystal. In addition, we conducted accelerated stability studies and hygroscopicity measurements to predict degradation behaviour and assess the potential for long-term storage under practical conditions. They are also reducing the costs compared to the classic stability studies, which are usually long-term and recommended by International Council for Harmonisation.[36] By focusing on the stability and degradation behaviour of CBD cocrystals, this study provides valuable insights into their potential as stable and effective solid forms for pharmaceutical development.

2 Materials and methods

2.1 Materials

View Article Online
DOI: 10.1039/D4CE01314J

Cannabidiol was purchased from PharmaHemp d.o.o (Ljubljana, Slovenia). The coformers (namely, 2,2′-bipyridine; 4,4′-bipyridine; 4-methylpyridin-N-oxide; L-arginine; caffeine; L-carnitine; L-cysteine; L-glutamic acid; L-glutamine; L-glycine; hippuric acid; indole; isonicotinic acid N-oxide; isonicotinamide; lidocaine; L-lysine; nicotinamide; L-phenylalanine; piperazine; polydatin; L-proline; pyridine-N-oxide; quercetin; riboflavin; tetramethylpyrazine; L-tryptophan; L-tyrosine; L-valine) were purchased from Sigma-Aldrich (St. Louis, USA) and were used as received. All coformers have purity higher than 98 %. Solvents such as methanol (MeOH), ethanol, cyclohexane (CHX), heptane (HP), and butyl acetate (BA) were purchased from PENTA (Prague, Czech Republic).

2.2 Screening and cocrystal preparation

The screening of CBD cocrystals was performed in a ratio 1:1 for all initial experiments. For the screening experiments, we selected 28 coformers based on the type of their functional groups (such as carboxylic, hydroxyl, alcohol), pKa, molecular size, and hydrogen-bonding propensity using Cambridge Structure Database (CSD). Some of the coformers used (e.g., caffeine, L-carnitine, L-proline) can be found in the GRAS database. To consider all these possible properties we also selected some coformers that are not pharmaceutically acceptable, such as 2,2′-bipyridine and 4,4′-bipyridine, but they can provide us further insight into the cocrystal formation and behaviour. This type of knowledge-based selection increases the probability of forming new cocrystals.[37] We also included five coformers, for which are reported CBD cocrystals in the patent literature.[24,25]

View Article Online
DOI: 10.1039/D4CE01314J

2.2.1 *Slurry experiments*

CBD (approximately 20 mg) and coformer were suspended in heptane or mixture of heptane and ethanol (ratio 95:5) in 2 ml vials. The slurry experiments were performed for 7 days at 25 °C and 750 rpm in a thermomixer. The obtained material was filtered and dried.

2.2.2 *Milling experiments*

Grinding experiments were carried out with a Retsch MM400 mixer mill. Approximately 50 mg of CBD and an equimolar amount of the coformer were mixed in a 2 ml polypropylene milling jar with two 5 mm stainless steel balls. Subsequently, a liquid additive (MeOH or HP) was added in an amount of 5 µl into the plastic jars which were immediately closed to prevent evaporation of the liquid additive. The milling experiments were carried out at a frequency of 25 Hz for 20 minutes.

2.2.3 *Single Crystal preparation*

The single crystal of CBD-BP was prepared by combining CBD and 4,4′-bipyridine in a 10:1 mixture of heptane and 1,4-dioxane, while CBD-PR was prepared in methanol. Both cocrystals were prepared by using CBD and the respective coformer in an equimolar ratio. These mixtures were heated to 35 °C to dissolve the powder and then left to cool down followed with slow evaporation until the single crystals were formed. The single crystals were consequently measured according to the conditions which are described below. The preparation of both single crystals did not present any challenges as opposed to the other forms. The crystal structure of the CBD-TMP cocrystal was not possible to be solved, because the single crystals were tiny needles with very low refractive index. Nevertheless, we tried to employ XRPD to solve its crystal structure. However, all attempts failed because of the crystal structure's broad diffraction profile and

View Article Online
DOI: 10.1039/D4CE01314J

complexity. We also tried to prepare single crystals of CBD-CR and CBD-PI by solvent evaporation or vapor diffusion, but all the experiments resulted in glassy oils. For this reason, we used the XRPD to determine the cocrystal structure. However, we succeeded to solve only the crystal structure of CBD-CR.

2.3 Characterization

2.3.1 Powder X-ray diffraction (XRPD)

The diffraction patterns were obtained for the raw powders and the prepared materials by a powder diffractometer X'Pert^3 Powder (PANanalytical, Holland) equipped with Cu anode Kα (λ = 1.542 Å) with a tube voltage of 40 kV and a tube current of 30 mA. The samples were measured from 4 to 40° 2θ with 0.026° 2θ step size and 56.87 s per step.

2.3.2 Single crystal and powder X-ray diffraction for the structure solution

The analysis of CBD-BP and CBD-PR was performed at 95 K using a SuperNova diffractometer with a micro-focus sealed tube, mirror-collimated Cu-Kα radiation (λ = 1.54184 Å), and CCD detector Atlas S2. The data reduction and absorption correction were done with CrysAlisPro software.[38] The structures were solved by charge flipping methods using Superflip software and refined by full matrix least squares on squared value using Crystals and Jana2020[39,40] software. MCE software was used for the visualization of residual electron density maps.[41] All H atoms were placed from residual electron density map and the C-H were constrained to ideal geometries. The single crystal sample of CBD-BP was twinned, and the structure was successfully solved from the main twin component. The structure of CBD-PR is slightly disordered, with one of the CBD side chains being in two positions with occupancies of 0.8 and 0.2.

View Article Online
DOI: 10.1039/D4CE01314J

The sample CBD-CR was ground and placed in the 0.5 mm borosilicate-glass capillary. Powder diffraction data was collected using the Debye-Scherrer transmission configuration on the powder diffractometer Smartlab of Rigaku (λCu, Kα1 = 1.54056 Å) that was equipped with a primary monochromator, focusing mirror, capillary holder and D/tex ultra 250 detector. XRPD pattern was measured from 3° to 80° 2Theta with a step size 0.01°. The overall measurement time was 20h. The structures were deposited into the Cambridge Structural Database under numbers 2333022 (CBD-BP), 2333083 (CBD-PR) and 2333084 (CBD-CR). Details of crystal structure solutions are in Supporting Information in Section SI 1.

2.3.3 Thermal analysis

Thermal properties were studied using differential scanning calorimetry DSC 3+ (Mettler Toledo, Switzerland) and thermogravimetric analysis (TGA). For DSC measurements, the aluminium pan was filled with 2 mg of sample. The aluminum pan was sealed and pierced to allow possible solvent vapour to escape and prevent an explosion. The investigation temperature range was from 20 °C to the specific degradation temperature of each sample, with a heating rate of 10 °C/min. In the TGA experiments, the pan was filled with approx. 2 mg of sample and heated from 30 °C to 300 °C with a heating rate of 5 °C/min. All measurements were carried out in the inert gas atmosphere.

2.3.4 Solution and solid-state nuclear magnetic resonance (NMR)

Solution NMR was utilized to determine the stoichiometry and purity of the prepared materials. The samples were dissolved in d_6-DMSO and the ^{1}H NMR spectra were measured by Avance III 500 MHz NMR spectrometer (Bruker, USA) equipped with a Prodigy probe and with a repetition delay of 10 s.

View Article Online
DOI: 10.1039/D4CE01314J

Solid-state NMR was used to confirm cocrystal creation and purity of the obtained material. The ^{13}C NMR spectra were measured by Avance III 400 MHz NMR spectrometer (Bruker, USA) equipped with a 4 mm probe and with 13 kHz spinning.

2.4 Intrinsic dissolution rate (IDR)

2.4.1 Preparation and measurement of IDR samples

The IDR was measured using Sirius inForm (Pion Inc., USA) connected to offline HPLC (High Performance Liquid Chromatography) detection. The IDR discs with a diameter of 3 mm filled with ca. 20 mg of sample were compressed with a constant load of 100 kg, relaxed for one minute, and compressed again with approximately 100 kg for the second minute. The intrinsic dissolution rate was measured in 40 ml of 0.01 M hydrochloric acid buffer solution (pH = 2.0) with the addition of 0.5% Tween 20 at 100 rpm. The samples for HPLC analysis were taken every two minutes in amount of 800 µl. After each sampling the taken amount was immediately replaced with fresh dissolution medium to maintain a constant volume. Each sample was measured in triplicate. IDR was calculated using a linear fit of the 40 minutes of the measurement. The first six minutes were excluded from the analysis, because they represent the first dissolution of the free non-compressed powder from the disc surface created during preparation. After each measurement, the discs underwent XRPD analysis to confirm the crystal structure of all samples and refute any potential changes in polymorphism.

2.4.2 HPLC analysis

The HPLC analysis was performed using Waters Alliance e2695 Separation Module (Agilent Technologies Inc., USA) with a high-pressure pump, an autosampler, a thermostat and a

View Article Online
DOI: 10.1039/D4CE01314J

photodiode-array detector. A Waters XBridge C18 column (Waters Corporation, USA) with dimension of 50 mm length and 4.6 mm internal diameter with particle size of 3.5 µm was used for the analysis of the released API. The autosampler temperature was set to 25 °C, the column heater was set up at 40 °C during analysis. Ultrapure water with addition of formic acid (0.1%) and acetonitrile was used as component A and B, respectively of the mobile phase for the separation. The gradient elution was set as follows: *t* (min)/% B: 0/30; 1.5/30; 6.5/80; 9/80; 9.5/30; 12/30 with the flow rate of the mobile phase 0.8 ml/min. The injection was set to 50 µl for each sample. For evaluation of the released amount of API, the absorbance at 210 nm was used. The chromatographic data were evaluated using the software Empower™.

2.5 Stability study

2.5.1 Preparation of samples for stability tests

Samples for stability measurements were prepared by weighing ca 50mg of pure CBD and each multicomponent form into 2 ml dark glass vials. Then, the samples were put into the dark stability chambers set to appropriate conditions. All powders were stored at 40 °C and 75 % relative humidity (RH) for 25 days, at 60 °C and 40 % or 75 % RH for 13 days, and at 80 °C and 40 % or 75 % RH for 3 days. All the samples were prepared in duplicate for each condition. After a specific time for each condition, the samples were taken from the chambers and analysed. The samples for UPLC (Ultra Performance Liquid Chromatography) measurement were diluted in methanol to a final concentration 1 mg/ml.

View Article Online
DOI: 10.1039/D4CE01314J

2.5.2 *UPLC purity analysis*

The UPLC analysis was performed using 1290 Infinity II LC System (Agilent Technologies Inc., USA) with a high-pressure pump, an autosampler, a thermostat and a diode array detector. An Acquity UPLC CSH Phenyl-Hexyl column (Waters Corporation, USA) with dimension of 150 mm length and 2.1 mm internal diameter with particle size of 1.7 µm was used for the purity analysis. The autosampler temperature was set to 5 °C, the column heater was set up at 20 °C during analysis. For the separation ultrapure water and acetonitrile was used as component A and B, respectively of the mobile phase. The gradient elution was set as follows: *t* (min)/*%* B: 0/50; 12/75; 14/100; 20/100; 20.5/50; 24/50. The flow rate of the mobile phase was 0.3 ml/min. The injection was set to 2 µl for each sample. The detection was performed using UV/Vis detector operated at a wavelength of 237 nm. The chromatographic data were evaluated using the software OpenLab CDS.

2.5.3 *Statistical analysis*

The data were processed by applying paired Student's significant test. The analysis focuses on calculation of *p*-values to determine the significance of the correlations between obtained data. We used three different significance levels (α = 0.1, 0.05, 0.01) for data description. The data with significant difference $p < 0.1$ are marked with *, $p < 0.05$ with **, $p < 0.01$ with ***, and are considered statistically significant.

2.5.4 *Dynamic vapour sorption analysis (DVS)*

The DVS isotherms for all phases and pure CBD were measured using SPS23-100n (ProUmid GmbH & Co. KG, Germany). The samples were exposed to a sorption cycle, and the relative humidity was gradually increased from 0% to 90% in steps of 10%. The weighing interval was 15

View Article Online
DOI: 10.1039/D4CE01314J

min. The minimum time per climate setting was 180 minutes, and the maximum was 30 hours, depending on the relative humidity level and the time required for the sample to reach equilibrium. The isotherms were measured at 25 °C.

2.5.5 Interaction Energies calculations (and Energy Frameworks)

Interaction energies and energy frameworks were calculated using the software CrystalExplorer17 version 17.5, revision f4e298a.[42] Molecular wave functions were obtained using the built-in Tonto utility at the "accurate" setting using the B3LYP/6-31G(d,p) level of theory. The pictures of the energy frameworks were created using the same software.

3 Results and discussion

3.1 Screening experiments

3.1.1 Slurry experiments

To initially confirm the formation of cocrystals obtained by slurry and milling experiments, the samples were analysed by XRPD. Four cocrystals were prepared by the slurry method, namely CBD-BP, CBD-PI, CBD-PR, and CBD-TMP out of 29 tried coformers. The comparison of the XRPD patterns of the CBD cocrystals obtained by slurrying compared to the input material and pure CBD is shown in Figure 2. For those with solved crystal structure, simulated XRPD patterns are also shown to confirm their phase purity. All prepared phases exhibited X-ray diffractograms that were different from those of the starting materials.

View Article Online
DOI: 10.1039/D4CE01314J

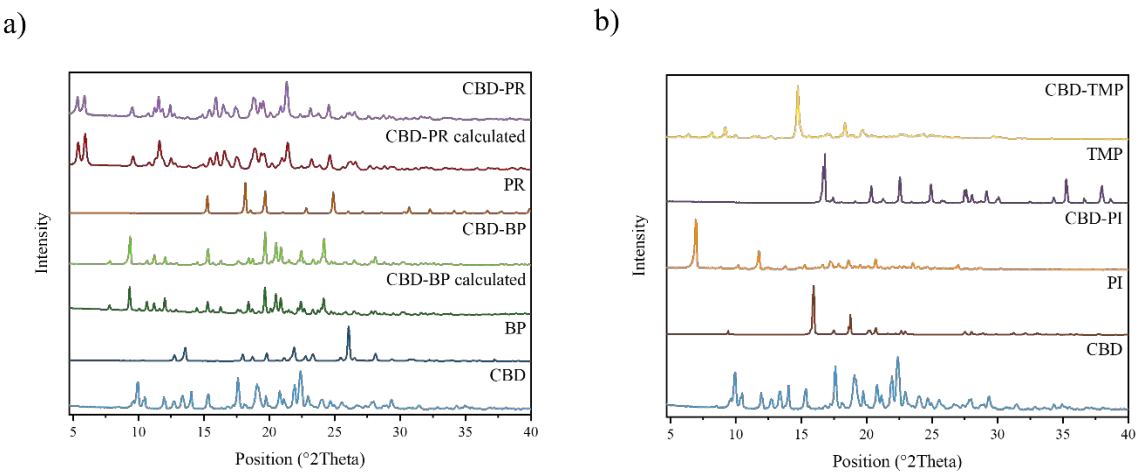

Figure 2. a) Experimental and calculated XRPD patterns of CBD-BP and CBD-PR cocrystals prepared by slurry compared to their starting materials b) experimental XRPD patterns of CBD-PI and CBD-TMP cocrystals compared to their starting material.

3.1.2 Milling experiments

The same set of coformers was used for mechanochemical screening. As a liquid additive, we used MeOH, which is polar and may behave as hydrogen donor or acceptor, and HP which is nonpolar. Liquid-assisted milling experiments may provide metastable forms of the same cocrystals or different cocrystals than the slurry method because more energy is applied to the system, and different interactions can be formed or broken.[43] Using the milling method, we successfully prepared the same cocrystals that were previously obtained with the slurry method, as described above.

The cocrystal with L-carnitine (CBD-CR) and betaine (CBD-BE) that were mentioned in the patent[24,25] were not within the positive results. To investigate if CBD-CR formation was possible under different conditions, we tried milling with the addition of butylacetate or cyclohexane as a liquid additive. In addition, we investigated different parameters as the ratio of the substances,

View Article Online
DOI: 10.1039/D4CE01314J

amount of liquid additive and period of milling. Although, in patent literature, the cocrystal is prepared using cyclohexane, we were able to prepare it only using 5 µl of BA, 1:1 ratio and a milling period of 100 min. The results of these experiments are shown in Figure 3. The XRPD patterns of the solids obtained from all solvents, except BA, matched the XRPD pattern of the pure API. By using different ratios of CBD and CR, we observed changes in the intensity of the first peak near 6.92 °2Θ. This peak is essential for the cocrystal, and it was getting less intense using higher ratio of CR. We can also observe the excess of CR in all ratios except 1:1 in positions, e.g., 18.88 and 22.08 °2Θ. We also attempted various conditions, including different solvents and ratios, to prepare CBD-BE in its pure cocrystal form. However, the resulting material consistently showed the excess of CBD. Thus, we did not involve this cocrystal in further characterization. During milling, no polymorphic changes of CBD were observed.

a)

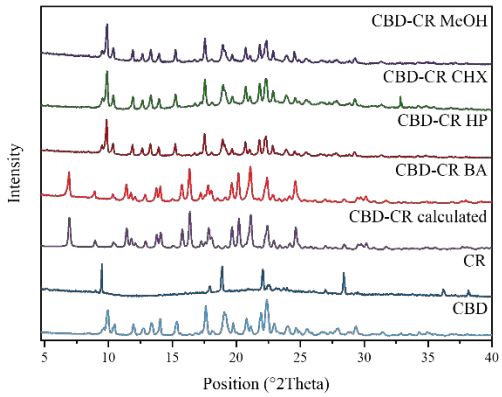

b)

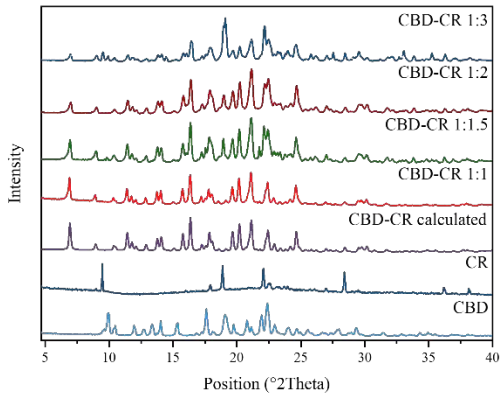

View Article Online
DOI: 10.1039/D4CE01314J

Figure 3. XRPD patterns of CBD-CR a) using different solvents, b) using different ratios.

The molar ratio of the prepared phases was further confirmed by ^{1}H NMR. It showed that the ratio of all prepared cocrystals was 1:1. The ssNMR was employed to provide further experimental evidence regarding the CBD cocrystals, confirming their formation by showing distinct changes in chemical shifts compared to the spectra of the input material. The ssNMR spectra can be found in Figure SI 2.

3.2 Characterization

3.2.1 Crystal structures and morphology of the solid forms

To confirm the CBD multicomponent forms and get an insight into the crystal structure and its interactions, we tried to prepare single crystals for each form by using the methods of slow solvent evaporation and vapour diffusion. Crystal structures were successfully solved for the cocrystals CBD-BP, CBD-CR, CBD-PR. The crystallographic data and details of refinement are presented in Section SI 1. For the solved structures we also predicted the Bravais−Friedel−Donnay−Harker (BFDH) morphology using software Mercury 2.0 in order to describe which functional groups are exposed to the crystal surface.

3.2.1.1 CBD

The crystal structure of pure CBD is known since 1977.[44,45] It crystallizes in the monoclinic system with the space group P 2_1. The asymmetric unit (Figure SI 3a) consists of two molecules of CBD and the unit cell (Figure 4a) is made in total by four molecules of CBD. The two molecules of CBD in the asymmetric unit are connected via oxygen atoms by a hydrogen bond (Figure SI 3b).

View Article Online
DOI: 10.1039/D4CE01314J

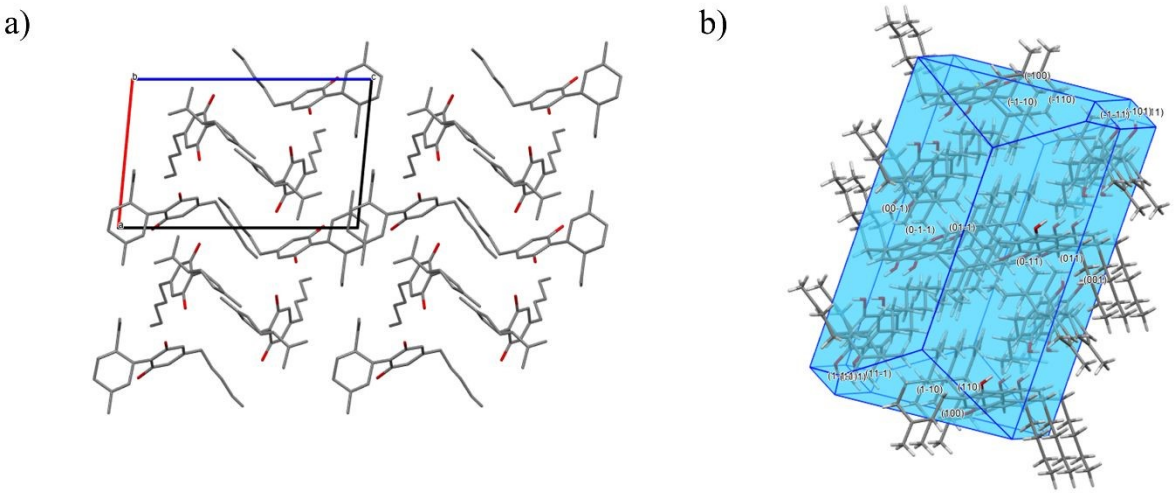

Figure 4. Crystal structure of CBD a) unit cell, b) predicted BFDH morphology.

The calculated interactions energy among two CBD molecules is −60.6 kJ/mol (Figure SI 3c). The BFDH predicted morphology of CBD (Figure 4b) is showing that on the crystal surface primarily exist the hydrophobic groups of CBD, which reduces the surface wettability.

3.2.1.2 CBD-BP

The CBD-BP cocrystal crystallized in a monoclinic system with the space group $P\ 2_1$. The asymmetric unit (Figure SI 4a) contains two molecules of CBD and two molecules of 4,4′-bipyridine, while in the unit cell (Figure 5a), there are four molecules of each kind. The hydrogen bond pattern (Figure SI 4b) is quite simple and bonds CBD with two molecules of 4,4′-bipyridine. The molecules of CBD create a channel to host the molecules of 4,4′-bipyridine. 4,4′-bipyridine molecules are arranged into layers and these layers are bonded by hydrogen bonding with CBD.

View Article Online
DOI: 10.1039/D4CE01314J

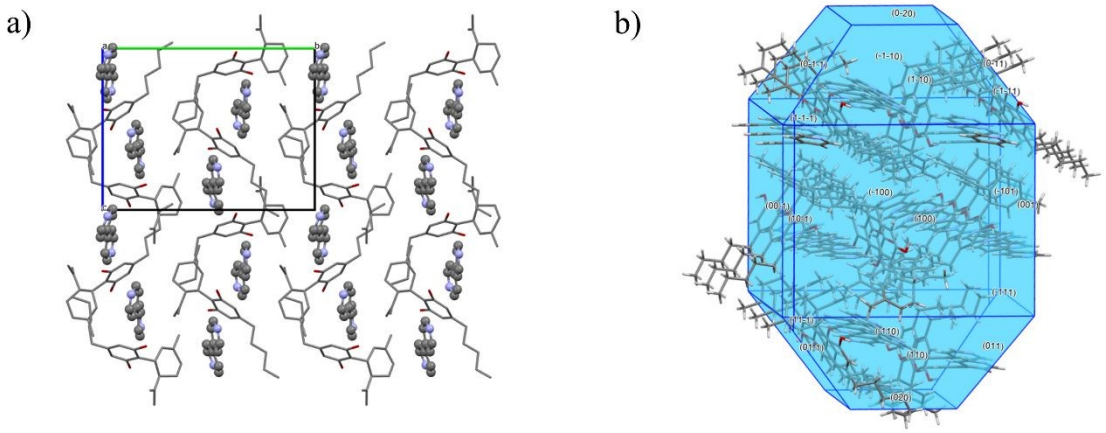

Figure 5. Crystal structure of CBD-BP of a) unit cell, b) predicted BFDH morphology.

The strongest interactions energy is approximately −47.5 kJ/mol and it is between the molecules of CBD and bipyridine (Figure SI 4c). The interaction energy between the molecules of CBD is a little bit lower, around −37.7 kJ/mol. The predicted BFDH morphology (Figure 5b) is showing that CBD exhibits its hydrophobic groups (aliphatic chain) in majority on the crystal surface. On the crystal surface there can be also found the hydrophilic groups of CBD, however, they are placed on the smaller faces. Hence, the cocrystal would be mostly behaving hydrophobic by itself.

3.2.1.3 CBD-CR

The cocrystal CBD-CR crystallizes in the orthorhombic system with $P\,2_12_12_1$ space group. In the asymmetric unit (Figure SI 5a), there is one molecule of each CBD and L-carnitine. The unit cell (Figure 6a) contains four molecules of each kind. The hydrogen bonding system (Figure SI 5b) is quite complex, and it involves bonding between CBD and L-carnitine and also within the molecule of L-carnitine between the carbonyl and hydroxyl group. The molecules of L-carnitine are located in the channels, which are created by the CBD molecules.

View Article Online
DOI: 10.1039/D4CE01314J

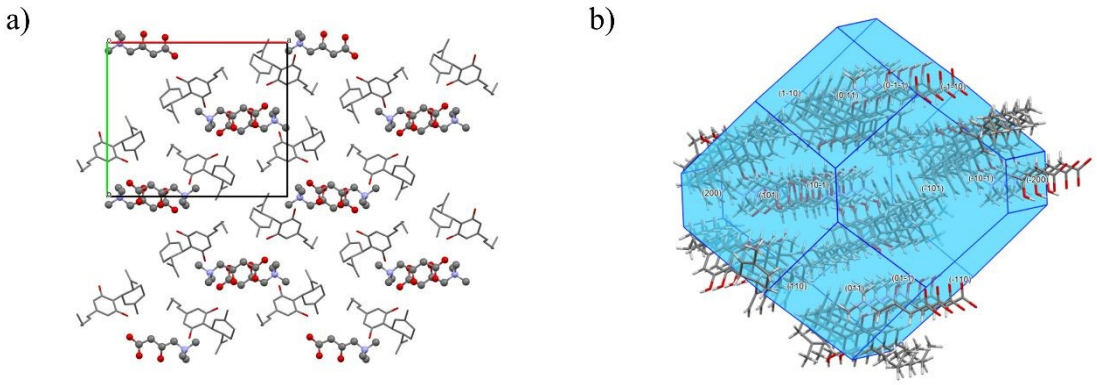

Figure 6. Crystal structure of CBD-CR of a) unit cell, b) predicted BFDH morphology.

The molecules of L-carnitine and CBD are connected with relatively weak interaction energies. The strongest of these interaction energies is approximately −23.8 kJ/mol (Figure SI 5c). The BFDH morphology (Figure 6b) is showing that mostly hydrophilic groups (carboxylic group of L-carnitine and hydroxy group of CBD) are exposed on the crystal surface of the cocrystal. This means that the cocrystal may easily interact with the atmospheric moisture, which may influence its physicochemical properties.

3.2.1.4 CBD-PR

The CBD-PR cocrystal has an orthorhombic symmetry with the space group $P\ 22_12_1$. In its asymmetric unit (Figure SI 6a), it has two molecules of CBD and two molecules of L-proline, which are in zwitterionic form. One molecule of CBD shows a disorder in the side aliphatic chain. The unit cell (Figure 7a) consists of 8 molecules of each CBD and PR. There are several hydrogen bonds in the crystal structure (Figure SI 6b). The most significant are four H-bonds between the CBD and L-proline molecules that are arranged in a square. The H-bonding connects L-proline

View Article Online
DOI: 10.1039/D4CE01314J

molecules together, by bonding NH and carbonyl group, as well as connects the CBD molecule with L-proline through carbonyl and hydroxyl group.

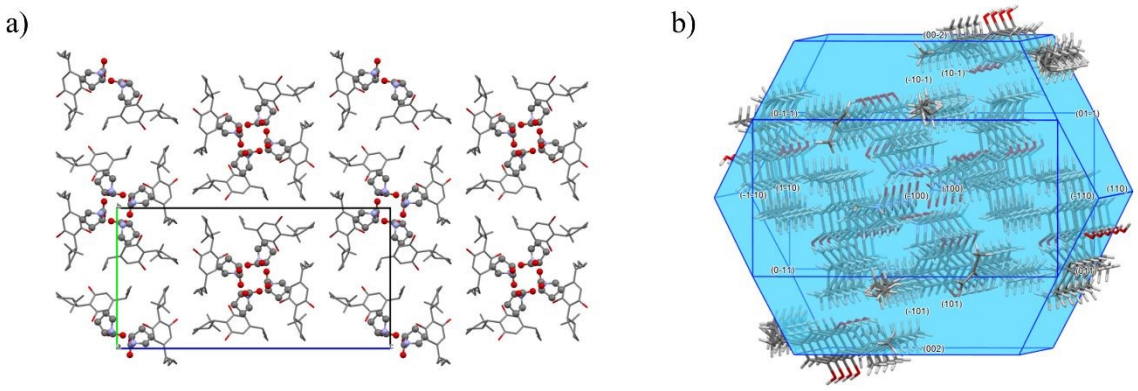

Figure 7. Crystal structure of CBD-PR of a) unit cell, b) predicted BFDH morphology.

The strongest interaction energy (Figure SI 6c) can be found between two molecules of CBD (approximately −36.8 kJ/mol), while there are also interactions between the molecules of CBD and L-proline, but they are under 20kJ/mol which is our cut off. The predicted BFDH morphology (Figure 7b) is showing both hydrophobic (aliphatic tail of CBD) and hydrophilic (hydroxy group of CBD) groups on the crystal surface of the cocrystal. However, the hydrophobic part shown on the surface is dominant.

3.3 Thermal analysis

Further characterization of the cocrystals in terms of their thermodynamic stability was provided by TGA and DSC analysis. The TGA and DSC results are shown in Figure 8. From the TGA curves (Figure 8a), a weight loss of approximately 34% for CBD-BP, 19% for CBD-PI and 27% for CBD-TMP is observed at temperatures near 180 °C, 160 °C and 100 °C, respectively. The weight loss is caused by the sublimation of the coformer in the cocrystal structure. However, as

View Article Online
DOI: 10.1039/D4CE01314J

shown in Figure SI 4, the coformers completely sublimate at approximately 160 °C, 130 °C and 100 °C, respectively, when not part of a cocrystal. The higher sublimation temperature observed for the coformers in cocrystal may result from interactions within the cocrystal structure, which probably require additional energy to overcome. For CBD-CR, a weight loss of 34 % is also observed at 180 °C, which is attributed to the partial degradation of the coformer alone. The observed weight losses align with the calculated molar mass percentages of the coformers in the cocrystals. The DSC and TGA curves of starting material compared to the cocrystals can be found in Section SI 4. Only in the case of the CBD-PR we do not see any weight loss while heating because L-proline is showing a higher thermal stability than the cocrystal itself.

From the DSC curves (Figure 8b) we can observe that the pure CBD shows the melting onset at 62 °C and a peak at 67 °C. In contrast, all new phases show higher melting points; CBD-PI melts at 85 °C (T_{onset}=77 °C), CBD-TMP at 93 °C (T_{onset}=90 °C), CBD-BP at 135 °C (T_{onset}=132 °C), CBD-PR at 149 °C (T_{onset}=140 °C) and CBD-CR at 153 °C (T_{onset}=147 °C). The last three mentioned cocrystals showed at least a double increase in the melting point compared to the pure CBD. However, for the samples CBD-BP, CBD-PI, and CBD-TMP, the melting event is accompanied by the decomposition of the coformer, which is shown in Figure 8a.

View Article Online
DOI: 10.1039/D4CE01314J

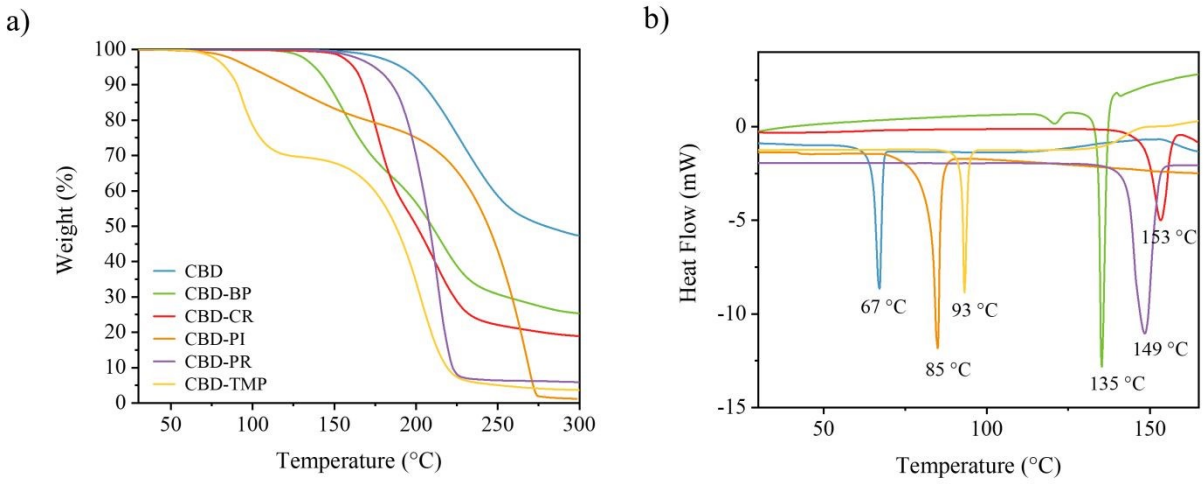

Figure 8. a) TGA thermograms and b) DSC thermograms of the CBD and the cocrystals CBD-BP, CBD-CR, CBD-PI, CBD-PR, and CBD-TMP.

The higher melting point of multicomponent solid forms is often believed to indicate higher thermal stability of the cocrystals. But when comparing melting temperature of the solid forms with their interaction energies, we can see that higher melting point does not always indicate higher interaction energies of the crystal. For example, for CBD-CR which has a melting point at 153 °C, we observed that it has relatively low energy between its molecules (−23.8 kJ/mol), which is the lowest compared to other cocrystals. In addition, CBD-BP with the third highest melting point (135 °C), still shows lower interaction energy between the molecules (−47.5 kJ/mol) compared to pure CBD (−60.6 kJ/mol), even though interaction energy between the molecules of CBD-BP is the highest between the cocrystals. This suggests that the stability of cocrystals in general is a more complicated property than we would expect, and it depends on many parameters such as the crystalline lattice arrangement, symmetry, interaction energies, hygroscopicity of the cocrystals etc.[46]

View Article Online
DOI: 10.1039/D4CE01314J

3.4 Dynamic vapour sorption

We performed as first the DVS analysis (Figure 9) to get further insight into the stability behaviour of the multicomponent solid forms when exposed to humidity. The stability of the cocrystals against atmospheric moisture is believed to be also connected to the crystal morphology.[47]

The pure CBD powder exhibited a low absorption of water even for high relative humidity, which is in accordance with its natural hydrophobicity.[1,14] The same hydrophobic behaviour as pure CBD was observed for cocrystal CBD-BP. The CBD-PR sample becomes slightly hygroscopic when exposed to relative humidity levels exceeding 80 %. The DVS results are in accordance with the predicted BFDH morphologies (Section 2.3.2) of these cocrystals. Both structures exhibit a higher number of hydrophobic groups on their crystal surfaces, which reduces their interaction with atmospheric moisture. On the other hand, CBD-TMP shows only decrease of the mass, which is connected to the tendency of tetramethylpyrazine to sublimate.[48] TMP by itself absorb water rapidly for RH ≥ 50 % (ref.[48]), however the formation of the cocrystal probably protects TMP to remain not hydrated even for high RH. The CBD-PI cocrystal shows also decrease of the mass up to 80 % RH, which is connected to the sublimation of PI, which occurs even under standard conditions.[49] The piperazine higher tendency of hygroscopicity[50] probably influences the behaviour of the cocrystal for higher (≥ 80 % RH) humidity, when it becomes slightly hygroscopic. Contrary to all multicomponent forms and pure CBD, the CBD-CR exhibits a high-water absorption for RH ≥ 50 %, the weight of the sample reached ca 63% for 90% RH. This high water absorption may be connected to the high hygroscopic tendency of L-carnitine, which was also

View Article Online
DOI: 10.1039/D4CE01314J

reported as a problem for tablet manufacturing due to the adhesion of tablets to punches.[51] Furthermore, the BFDH morphology prediction is showing mostly hydrophilic groups on the crystal surface, which are probably easily interacting with the atmospheric moisture.

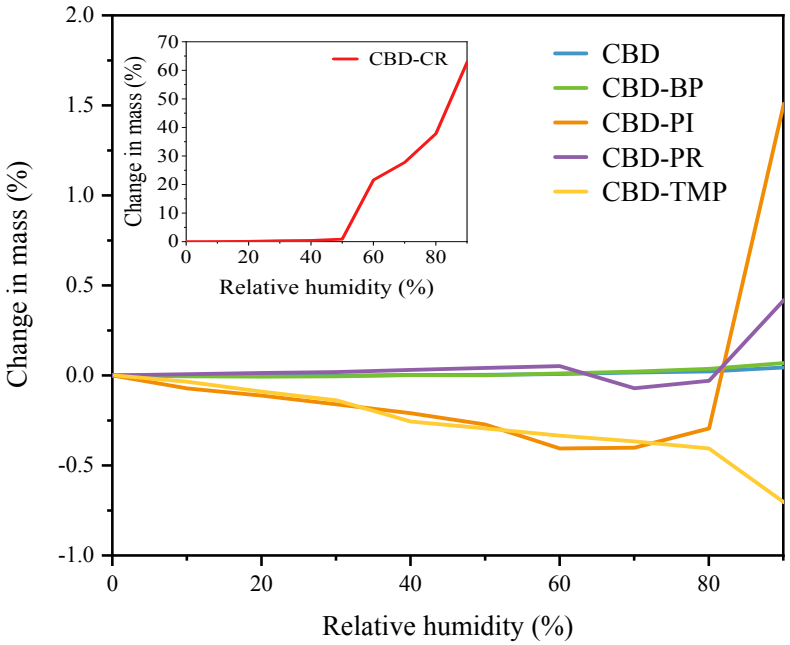

Figure 9. The DVS curves of CBD and its cocrystals.

3.5 Intrinsic dissolution rate

The IDR measurements were performed for pure CBD and its cocrystals. The dissolution study was carried out in hydrochloride acid buffer (pH=2) to mimic the environment of the stomach. The results are shown in Section SI 5, along with the exact IDR values and the dissolution rate profiles for all cocrystals and pure CBD. All the cocrystals showed lower IDR value than pure CBD (13.05 ± 0.32 $\mu g \cdot min^{-1} \cdot cm^{-2}$).

View Article Online
DOI: 10.1039/D4CE01314J

To gain further insight into the dissolution mechanism, we performed XRPD analysis of the disks after dissolution (Figure SI 11). In all cases, we observed peaks of cocrystals together with the pure CBD suggesting partial transformation of cocrystals after exposure to the water environment. The observed transformation of the cocrystals might be connected to weak interaction energies between the molecules of CBD and coformers and the hydrophilic nature of the coformers, which contain polar functional groups. The combination of these factors suggests that the cocrystals are unstable in an aqueous environment, leading to their dissociation into the coformer and CBD. Thus, CBD becomes available for dissolution only after this dissociation process occurs. Given that cocrystal decomposition follows a kinetic pathway, this phenomenon likely contributes to the slightly slower dissolution rates observed for the cocrystals (Figure SI 9). This hypothesis is further supported by the behaviour of CBD-CR, where its more hydrophilic surface coupled with low interaction energy (−23.8 kJ/mol) is allowing easier contact of the cocrystal with water and faster decomposition, therefore resulting in higher IDR compared to other cocrystals.

3.6 Stability and degradation studies

The stability and degradation studies were performed to describe the behaviour of the multicomponent solid forms compared to the pure CBD under accelerated storing conditions. We analysed the amount of CBD in the samples, checked the visual changes (colour and state of the powder) and the crystalline state after removing the samples from stability chambers. All the samples before the accelerated stress study were white powders, except CBD-PI which was originally brownish. The results are showed in Figure 10.

View Article Online
DOI: 10.1039/D4CE01314J

As can be seen, pure CBD showed a considerable difference in the CBD amount in each case except storage in 40 °C/75 % RH and 60 °C/75 % RH where it remained stable, confirmed by both UPLC and XRPD analysis (Figure SI 12a). However, the sample stored at 60 °C/40 % RH and at 80 °C, showed a higher decrease in purity of CBD, and furthermore the samples changed into jelly-like state with brownish colour, which is caused by the fact that the storage conditions are close or even exceeding the melting point of CBD.

For the CBD-BP cocrystal no significant decrease of CBD was observed, and it remained stable the whole time of the experiment under different conditions. Furthermore, the stability of the sample in each condition was confirmed using XRPD (Figure SI 12b); all the samples remained in powder unchanged state.

Storing CBD-CR at 40 °C/75 % RH for 25 days did not cause any decrease in the amount of CBD. However, XRPD analysis confirmed a change in the solid state of the sample (Figure SI 12c). The XRPD pattern shows almost the same peaks as pure CBD, but we can also identify peaks belonging to L-carnitine (e.g., 9.46, 17.94, 18.89 °2Θ). This observation suggests that after storing, the cocrystal is starting to get disintegrated to the initial compounds. Under the 60 °C/40 % RH conditions, only a slight decrease in CBD amount was observed, and the cocrystal pattern remains preserved, as shown by the XRPD results. Storing CBD-CR under remaining conditions led to a significant decrease in CBD amount, and the samples also deliquesced. These results, combined with the DVS data, becomes evident that L-carnitine exhibits high water absorption. It can be assumed that the stability of CBD-CR is also highly dependent on the applied relative humidity.

View Article Online
DOI: 10.1039/D4CE01314J

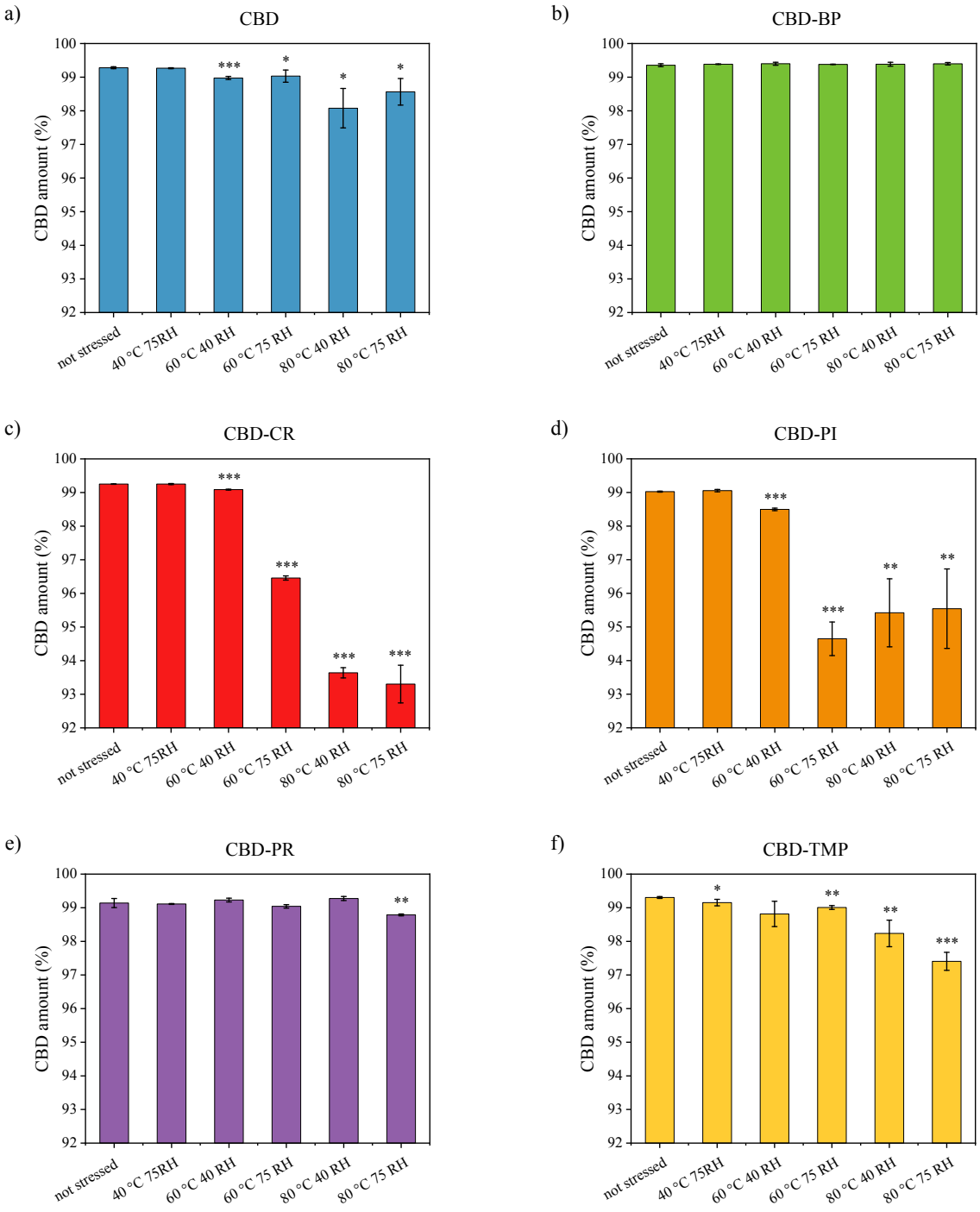

Figure 10. The CBD amount in the not stressed cocrystals and pure CBD compared to the CBD amount for the cocrystals and pure CBD after accelerated stressed conditions.

View Article Online
DOI: 10.1039/D4CE01314J

CBD amount in the sample CBD-PI remained stable while storing in 40 °C/75 % RH, furthermore the solid state remained stable according to XRPD (Figure SI 12d). The rest of the used conditions led to a statistically significant decrease in the amount of CBD. The samples stored at 60 °C and 80 °C were changed into jelly-like state after removing them from the chambers. This may be caused by the fact that the storage temperature is close to its melting point.

When samples of CBD-PR were stored at all conditions, the CBD amount and the crystalline state remained stable, except the sample stored at 80 °C/75 % RH. In that case the colour of the sample changed into a darker beige colour, which may be connected to the water adsorption in the environment with extreme conditions. Nevertheless, the XRPD analysis (Figure SI 12e) confirmed the initial cocrystal state.

The CBD-TMP showed a decrease in the amount of CBD while stored under different conditions. The sample stored at 60 °C/40 % RH changed its colour to red, however the cocrystal formation was still preserved, which was confirmed by XRPD (Figure SI 12f). When storing the sample at 60 °C/75 % RH, the XRPD analysis confirmed a change of the solid state. The XRPD pattern showed new peaks e.g., at 9.65, 10.14, 15.02 °2Θ corresponding to the pure CBD; however, there are still preserved some peaks corresponding to the cocrystal formation (e.g., 8.95, 14.50, 18.10 °2Θ). Therefore, we can expect the CBD-TMP is partially disintegrated into initial compounds, but part of the cocrystal is still preserved. Both samples stored at 80 °C were transformed into a jelly-like state, with a brown colour.

Overall, regarding the stability of multicomponent forms, the cocrystals with 4,4′-bipyridine and L-proline showed higher stability than the rest of the solid forms. Furthermore, they remained in a

View Article Online
DOI: 10.1039/D4CE01314J

powder state throughout the entire storage period. We did not observe any melting or deliquescence, or water sorption of the powder. The high stability may be caused by the fact that in the BFDH morphology prediction the crystal is showing mostly hydrophobic parts on the surface, which are probably protecting the cocrystal from interacting with the atmospheric moisture and to accelerate its disintegration. For the remaining cocrystals, we expect that humidity primarily influences their stability, rather than heat, because we observed their tendency to deliquesce even under conditions below their corresponding melting point. In the case of CBD-CR the stability is mainly influenced by its crystal morphology, which is exhibiting mostly with the hydrophilic groups on the crystal surface. These groups may interact with the atmospheric humidity and probably turn faster the degradation of the cocrystal, although the cocrystal is showing the highest melting point (153 °C). Furthermore, the calculation of interaction energies for the available crystal structures confirmed our observation, e.g., in the case of CBD-CR we obtained the lowest interaction energies (−23.8 kJ/mol) compared to the cocrystals with 4,4′-bipyridine (−47.5 kJ/mol) or L-proline (−36.8 kJ/mol) and resulting in faster disintegration of the cocrystal. Apart the already mentioned reasons, there are other ones that might accelerate and turn lower the stability of the cocrystal, such as higher surface area of the crystal or appearance of pores in the structure.

Regarding the degradation of the cocrystals, we could observe the same phenomenon as for the stability behaviour of the cocrystals. It means that the new solid forms with 4,4′-bipyridine and L-proline are protected from degradation by their high stability. On the other hand, the rest of the cocrystals are showing faster degradation, because of lower stability of the cocrystal. Hence, we

View Article Online
DOI: 10.1039/D4CE01314J

assume according to performed analyses, that the cocrystals are firstly disintegrated and consequently degraded by the applied humidity and heat.

4 Conclusion

In this study, we explored the synthesis and characterization of five CBD cocrystals, with the aim to investigate their physicochemical properties. Thermal analysis revealed that all cocrystals demonstrated higher melting points compared to the pure CBD. It was found that the intrinsic dissolution rate of the cocrystals was slightly lower in all cases compared to the free CBD. This behaviour is probably due to their instability in an aqueous solution and their rapid dissociation, caused by low interaction energies between the CBD and coformer in combination with hydrophilic nature of the coformers. To investigate further the stability of cocrystals, we performed stability studies of all cocrystals and pure CBD under different humidity and temperature conditions. Among the tested cocrystals CBD-4,4′-bipyridine, which did not exhibit the highest melting point, demonstrated the highest stability, showing no significant degradation under stress conditions. However, its potential in pharmaceutical applications is limited because 4,4′-bipyridine is not considered a pharmaceutically acceptable compound. CBD-L-proline also exhibited notable stability, likely due to its hydrophobic crystal surface and strong molecular interactions within the cocrystal. Our results emphasize that melting point is not the sole determining factor for the stability of the cocrystals. It is important to consider also other factors, such as interaction energies of the molecules, surface morphology and hygroscopicity of the crystals. The demonstrated stability improvements in the cocrystal CBD-L-proline, suggests its potential for further development as solid-state form in pharmaceutical applications. Future research could explore

View Article Online
DOI: 10.1039/D4CE01314J

optimization of the processing conditions to obtain this cocrystal in larger quantities. Additionally, in vivo studies could be conducted to reveal the therapeutic efficacy.

Data availability

Additional data are provided in the ESI file. Crystallographic data for 2333022 (CBD-BP), 2333083 (CBD-PR) and 2333084 (CBD-CR) has been deposited at the Cambridge Structural Database.

Conflicts of interest

There are no conflicts to declare.

Acknowledgement

We would like to acknowledge the Pharmaceutical Applied Research Centre (PARC) for support in various part of this project and providing necessary instruments. The authors would also like to thank Jakub Heřt and Marcela Tkadlecová. for support and discussion. This work was supported by the grant from Czech Health Research Council (NU22-08-00346).

CRediT authorship contribution statement

Adéla Koryťáková - Conceptualization, Methodology, Investigation, Writing – original draft.

Argyro Chatziadi - Conceptualization, Methodology, Investigation, Writing – review & editing.

Jan Rohlíček - Methodology, Investigation, Writing – review & editing.

Eliška Zmeškalová - Methodology, Investigation, Writing – review & editing.

Josef Beránek - Conceptualization, Methodology, Supervision, Writing – review & editing.

View Article Online
DOI: 10.1039/D4CE01314J

Miroslav Šoóš - Conceptualization, Methodology, Supervision, Writing – review & editing, Funding acquisition.

5 Literature

Uncategorized References

1. L. Grifoni, G. Vanti, R. Donato, C. Sacco and A. R. Bilia, *Molecules*, 2022, **27**, 6070.
2. M. M. Radwan, S. Chandra, S. Gul and M. A. ElSohly, *Molecules*, 2021, **26**, 2774.
3. E. M. Williamson and F. J. Evans, *Drugs*, 2000, **60**, 1303-1314.
4. N. Peyravian, S. Deo, S. Daunert and J. J. Jimenez, *ImmunoTargets Ther.*, 2020, DOI: https://doi.org/10.2147/ITT.S263690 131-140.
5. B. Stella, F. Baratta, C. Della Pepa, S. Arpicco, D. Gastaldi and F. Dosio, *Drugs*, 2021, **81**, 1513-1557.
6. A. Fraguas-Sanchez, A. Fernández-Carballido, C. Martin-Sabroso and A. Torres-Suárez, *J. Chromatogr. B*, 2020, **1150**, 122188.
7. Epidyolex, https://www.ema.europa.eu/en/medicines/human/EPAR/epidyolex, (accessed 02.01.2024).
8. Sativex, https://www.ema.europa.eu/en/medicines/human/paediatric-investigation-plans/emea-000181-pip02-13-m01, (accessed 02.01.2024).
9. K. Knaub, T. Sartorius, T. Dharsono, R. Wacker, M. Wilhelm and C. Schön, *Molecules*, 2019, **24**, 2967.
10. S. A. Millar, R. F. Maguire, A. S. Yates and S. E. O'Sullivan, *Pharmaceuticals*, 2020, **13**, 219.
11. K. Hatziagapiou, K. Bethanis, E. Koniari, E. Christoforides, O. Nikola, A. Andreou, A. Mantzou, G. P. Chrousos, C. Kanaka-Gantenbein and G. I. Lambrou, *Pharmaceutics*, 2022, **14**, 706.
12. G. P. Andrews, *Philos. Trans. R. Soc., A*, 2007, **365**, 2935-2949.
13. Z. B. Shariff, D. T. Dahmash, D. J. Kirby, S. Missaghi, A. Rajabi-Siahboomi and I. D. Maidment, *J. Am. Med. Dir. Assoc.*, 2020, **21**, 1015-1023.
14. S. A. Millar, N. L. Stone, A. S. Yates and S. E. O'Sullivan, *Front. Pharmacol.*, 2018, **9**, 1365.
15. K. Mozaffari, S. Willette, B. F. Lucker, S. E. Kovar, F. O. Holguin and I. Guzman, *Molecules*, 2021, **26**, 3573.
16. P. Guruprasad Reddy, A. Bar-Hai, A. Hoffman, S. Marc Feldmann and A. J. Domb, *Bioorg. Chem.*, 2023, **141**, 106914.
17. O. Jennotte, N. Koch, A. Lechanteur and B. Evrard, *J. Drug Delivery Sci. Technol.*, 2022, **71**, 103372.
18. N. Koch, O. Jennotte, Y. Gasparrini, F. Vandenbroucke, A. Lechanteur and B. Evrard, *Int. J. Pharm.* , 2020, **589**, 119812.
19. H. E. Straker, L. McMillan, L. Mardiana, G. R. Hebberd, E. Watson, P. G. Waddell, M. R. Probert and M. J. Hall, *CrystEngComm*, 2023, **25**, 2479-2484.
20. N. Schultheiss and A. Newman, *Cryst. Growth Des.*, 2009, **9**, 2950-2967.
21. M. Guo, X. Sun, J. Chen and T. Cai, *Acta Pharm. Sin. B*, 2021, **11**, 2537-2564.
22. N. Qiao, M. Li, W. Schlindwein, N. Malek, A. Davies and G. Trappitt, *Int. J. Pharm.* , 2011, **419**, 1-11.
23. N. Shan and M. J. Zaworotko, *Drug Discovery Today*, 2008, **13**, 440-446.

View Article Online
DOI: 10.1039/D4CE01314J

24. US10604467B2, 2020.
25. WO2019030158A1, 2019.
26. B. K. Kalita, D. Pathak, H. Sharma and B. Sarma, *Stud. Nat. Prod. Chem.*, 2023, **78**, 323-364.
27. Proprietary CBD:TMP Cocrystal for Anxiety & Depression, https://artelobio.com/pipeline/art12-11/, (accessed 18.07.2024).
28. R. Mechoulam and L. r. Hanuš, *Chem. Phys. Lipids*, 2002, **121**, 35-43.
29. J. Yangsud, S. Santasanasuwan, P. Ahkkarachinoreh, A. Maha, F. Madaka, J. Suksaeree, T. Songsak, A. Vutthipong and C. Monton, *Adv. Tradit. Med.*, 2021, **21**, 475-484.
30. W. Jaidee, I. Siridechakorn, S. Nessopa, V. Wisuitiprot, N. Chaiwangrach, K. Ingkaninan and N. Waranuch, *Cannabis Cannabinoid Res.*, 2021, **7**, 537-547.
31. C. Franco, S. Protti, A. Porta, F. Pollastro, A. Profumo, B. Mannucci and D. Merli, *Results Chem.*, 2022, **4**, 100465.
32. H. Zheng, B. Chen and J. Rao, *Food Funct.*, 2022, **13**, 4502-4512.
33. V. N. Tran, O. Strnad, J. Šuman, T. Veverková, A. Sukupová, P. Cejnar, R. Hynek, O. Kronusová, J. Šach, P. Kaštánek, T. Ruml and J. Viktorová, *Int. J. Pharm.* , 2023, **643**, 123202.
34. K. B. Scheidweiler, M. Andersson, M. J. Swortwood, C. Sempio and M. A. Huestis, *Drug Test. Anal.*, 2017, **9**, 143-147.
35. E. Kosović, D. Sýkora and M. Kuchař, *Pharmaceutics*, 2021, **13**, 412.
36. O. González-González, I. O. Ramirez, B. I. Ramirez, P. O'Connell, M. P. Ballesteros, J. J. Torrado and D. R. Serrano, *Pharmaceutics*, 2022, **14**, 2324.
37. M. Singh, H. Barua, V. G. S. S. Jyothi, M. R. Dhondale, A. G. Nambiar, A. K. Agrawal, P. Kumar, N. R. Shastri and D. Kumar, *Pharmaceutics*, 2023, **15**, 1161.
38. CrysAlisPro, *Journal*, 2014.
39. V. Petříček, L. Palatinus, J. Plášil and M. Dušek, *Z. Kristallogr. Cryst. Mater.*, 2023, **238**, 271-282.
40. L. Palatinus and G. Chapuis, *J. Appl. Crystallogr.*, 2007, **40**, 786-790.
41. J. Rohlíček and M. Hušák, *J. Appl. Cryst.*, 2007, **40**, 600-601.
42. C. F. Mackenzie, P. R. Spackman, D. Jayatilaka and M. A. Spackman, *IUCrJ*, 2017, **4**, 575-587.
43. A. Chatziadi, E. Skořepová, J. Rohlíček, M. Dušek, L. Ridvan and M. Šoóš, *Cryst. Growth Des.*, 2020, **20**, 139-147.
44. P. G. Jones, L. Falvello, O. Kennard, G. Sheldrick and R. Mechoulam, *Acta Crystallogr., Sect. B: Struct. Crystallogr. Cryst. Chem.*, 1977, **33**, 3211-3214.
45. T. Ottersen, E. Rosenqvist, C. Turner and F. El-Feraly, *Acta Chemica Scandinavica B*, 1977, **31**, 807-812.
46. A. Chatziadi, E. Skorepova, J. Jirat, J. Rohlíček and M. Šoóš, *Cryst. Growth Des.*, 2022, **22**, 3395-3404.
47. R. Thakuria, M. Arhangelskis, M. D. Eddleston, E. H. H. Chow, K. K. Sarmah, B. J. Aldous, J. F. Krzyzaniak and W. Jones, *Org. Process Res. Dev.*, 2019, **23**, 845-851.
48. Y. Xie, L. Gong, Y. Tao, B. Zhang, L. Zhang, S. Yang, D. Yang, Y. Lu and G. Du, *Molecules*, 2024, **29**, 2208.
49. L. Zaharani, M. R. Johan and N. G. Khaligh, *J. Therm. Anal. Calorim.*, 2022, **147**, 14183-14193.
50. X. Wang, S. Xu, L. Jia, Y. Yang, Y. Liu, J. Gong and S. Wu, *CrystEngComm*, 2019, **21**, 5284-5291.
51. A. A. Badawi, M. M. Hegazy, D. Louis and M. A. Eldegwy, *Acta Pharm.* , 2017, **67**, 511-525.

View Article Online
DOI: 10.1039/D4CE01314J

Footnote

Electronic supplementary information (ESI) available: Crystal structure data for 2333022 (CBD-BP), 2333083 (CBD-PR) and 2333084 (CBD-CR) , NMR spectra, TG and DSC curves, XRPD after accelerated stability study.

View Article Online
DOI: 10.1039/D4CE01314J

Data availability

Additional data are provided in the ESI file. Crystallographic data for 2333022 (CBD-BP), 2333083 (CBD-PR) and 2333084 (CBD-CR) has been deposited at the Cambridge Structural Database.